2 Conf-921103--6-Rev.1

UCRL-JC-111286 Rev. 1
PREPRINT

Laser Driven Hydrodynamic Instability Experiments

B. Remington, S. Weber, S. Haan, J. Kilkenny, S. Glendinning,
R. Wallace, W. Goldstein, B. Wilson, and J. Nash

This paper was prepared for submittal to
34th Annual APS Meeting of the Division of the Plasma Physics
November 16-20, 1992, Seattle, WA

February 17, 1993

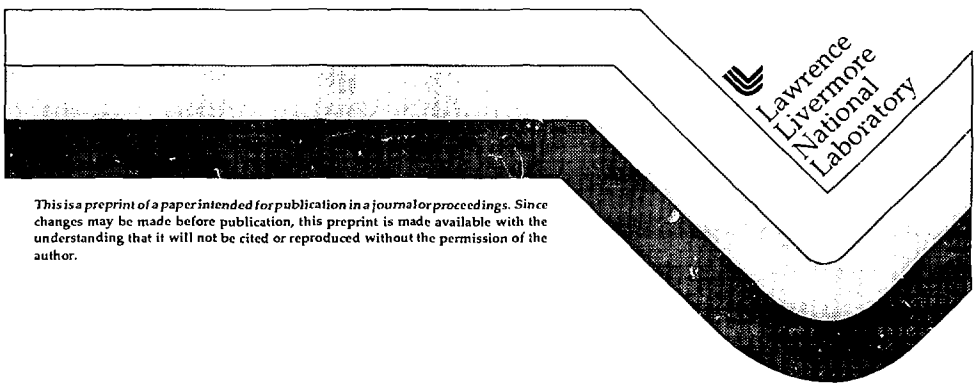

Laser Driven Hydrodynamic Instability Experiments

B.A. Remington, S.V. Weber, S.W. Haan, J.D. Kilkenny, S.G. Glendinning,
R.J. Wallace, W.H. Goldstein, B.G. Wilson, and J.K. Nash

Lawrence Livermore National Laboratory
Livermore, CA 94550

Abstract

An extensive series of experiments has been conducted on the Nova laser to measure hydrodynamic instabilities in planar foils accelerated by x-ray ablation. Single mode experiments allow a measurement of the fundamental growth rates from the linear well into the nonlinear regime. Two-mode foils allow a first direct observation of mode coupling. Surface-finish experiments allow a measurement of the evolution of a broad spectrum of random initial modes.

PACS 52.35.Py, 52.70.-m, 52.65.+65.+z

I. Introduction

The configuration of a high density fluid sitting on top of a low density fluid is Rayleigh-Taylor[1] unstable. Random perturbations at the interface between the two fluids will grow, with fingers (or "spikes") of the heavier fluid poking through the lighter fluid, and bubbles of the lighter fluid rising into the heavier fluid. Unfortunately, this situation occurs in the field of inertial confinement fusion (ICF), since the basic mechanism of driving an

implosion by ablating the outer layers of a spherical capsule is inherently RT unstable, independent of the details of the drive. Perturbations at the ablation front, whether initiated by capsule surface imperfections or by laser hot spots, will grow, possibly leading to shell breakup or degraded imlosion performance.[2]

A number of experiments have been done in direct drive,[3] that is, where laser light directly illuminates the accelerating surface, to measure the amount of perturbation growth on ablatively accelerated foils. Our work is the only active experimental RT effort that we are aware of for indirect drive, where the laser light is first converted to x-rays in a high-Z case called a hohlraum. We report here on a series of RT experiments with planar foils[4-6] of fluorosilicone (FS) and CH(Br), using a shaped, low adiabat x-ray drive. In Sec. II we describe the experimental setup, and in Sec. III we present results from single-mode experiments and simulations. We discuss our two-mode experiments in Sec. IV, and present an initial set of data from very recent surface-finish experiments in Sec. V. A summary and conclusion is given in Sec. VI.

II. EXPERIMENTAL SETUP

Surface perturbations are imposed on one side of a 750 μm diameter FS ($SiOC_4H_7F_3$) or CH(Br) foil (specifically, $C_{50}H_{47}Br_{2.7}$) and mounted across a diagnostic hole on the wall of a Au hohlraum with perturbation facing inwards, as illustrated in Fig. 1a. The foil is accelerated as shown schematically in the figure for face-on geometry. Side-on geometry is similar, except with the hohlraum rotated about its axis of symmetry by 90°. In face-on experiments, the growing modulations in the foil areal density translate to modulations in transmitted backlighter x-rays. In side-on geometry, the foil position is imaged as an edge-on shadow in the

backlighter x-rays. One-dimensional (1D) imaging is accomplished either with a streaked 22X magnification Wölter x-ray microscope[7,8] (the "22X") or with a new 20X magnification streaked-slit imager.[9] Two-dimensional (2D) x-ray imaging is accomplished with a gated x-ray pinhole camera.[10]

The drive was generated by focussing eight λ=0.351 μm, 2.1 kJ, 3.2 ns shaped Nova[11] beams into a gold cylindrical hohlraum, which then convert to x-rays as shown in Fig. 1a. The drive laser pulses have a low intensity, ~1.5-ns foot followed by a rapid increase to peak power at ~2.6-3.0 ns, with the peak/foot intensity ratio being 10-20, as shown in Fig. 1b. This generic shape is designed to keep the foil on a low adiabat, that is, high compression with a minimum of shock heating. The foil was backlit with a large area spot of x-rays created by irradiating a backlighter disk of Mo, Rh, Sc, or Fe (depending on the experiment) with a ninth Nova beam of wavelength, shape, and energy of 0.53 μm, 5.0 ns square, and 2.5 kJ, respectively. When combined with the filter and detector responses, the measured backlighter emission spectra were dominated by 2.3-2.9 keV and 2.7-3.2 L-band $3\rightarrow 2$ transitions for Mo and Rh (the Rh spectrum is given in Fig. 4, ref. 5) and 4.3 keV and 6.7 keV He_α K lines for Sc and Fe, respectively. In all cases the backlighter spectrum has been measured on separate Nova shots under similar laser conditions. On the surface finish experiments, where the long-range (~300 μm) backlighter structure might interfere with the interpretation of the data, a random phase plate (RPP) was used to generate a smooth backlighter profile. (See Figs. 2b and 3 in ref. 8 for an example of the smooth $\text{sinc}^2 x$ backlighter profile resulting from an RPP-smoothed Nova beam incident on a Mo disk and imaged in 2D with the 22X.)

To illustrate the gross hydrodynamics of a foil ablatively accelerated with a shaped drive, we show in Fig. 1c a streaked image of a foil trajectory experiment using a CH(Br) foil. This side-on measurement tracks the

shadow of the foil viewed edge-on; the data shown in Fig. 1d represent a combination of three such shots, using either the streaked slit[9] or the 22X.[7,8] We show with the solid curve the result of the 1D LASNEX[12] simulation, and the agreement with the measured foil position is quite good. We also include the time-dependent acceleration, density gradient scale length ($L = \rho/\Delta\rho$), and ablation velocity [$v_a = \dot{m}/(\rho \cdot \text{Area})$] from the simulation.

III. SINGLE-MODE EXPERIMENTS

To illustrate the basic features of a perturbation growth experiment, we show in Fig. 2 the result of gated 2D x-ray images in side-on geometry of *an accelerated FS foil containing a* $\lambda = 100\ \mu m$, $\eta_0 = 4.5\ \mu m$ *sinusoidal* perturbation. Early in time (2.0 ns) the perturbation is still sinusoidal, indicating the linear regime of RT growth. At 3.2 ns the foil is quite compressed and showing the first signs of deviation from a pure sinusoidal shape. By 4.4 ns, the foil has evolved into the classic bubble-and-spike shape characteristic of the nonlinear Rayleigh-Taylor regime. Within the ~10 μm spatial resolution of the instrument, we see no evidence of Kelvin-Helmholtz (KH) mushrooming in the spike tips. The result of the 2D simulation at 4.4 ns, given in Fig. 2d, also shows no KH tip broadening, even prior to folding with the experimental resolution function. The comparison of simulation with the data shown in Figs. 2c and 2d shows good qualitative agreement. We also observed late in time (4.4 ns) indications of foil bowing (not shown), suggesting that the edges of the foil see slightly less drive than the central region. This shadowing was accentuated on this particular shot by the way the foil was mounted on a Be washer to allow the ablation front to be easily observed. Nevertheless, as a matter of practice we omit the edge regions of the foils when extracting quantitative results in face-on geometry. (An indication of shadowing in face-on geometry can be seen by

the delayed burn through at the edges in Fig. 3 of ref. 4 or Fig. 6 or ref. 5.) No attempt is made to include shadowing in the simulations.

Perturbation growth is more quantitatively studied using face-on radiography, as shown in Fig. 3. A streaked image of a CH(Br) foil containing a λ=100 μm, η_0=2.5 μm sinusoidal initial perturbation is shown in Fig. 3a. Profiles on ln(Exposure) at early (0.2 ns), intermediate (2.2 ns), and late (4.2 ns) times are shown in Fig. 3b, and their corresponding Fourier spectral compositions are given in Fig. 3c. Early in time (0.2 ns) the initial perturbation appears sinusoidal in ln(Exposure)$\propto$optical depth. By t=2.2 ns, the perturbation has grown but is still sinusoidal, indicating that the evolution is in the linear regime and growing according to $\eta=\eta_0 e^{\gamma t}$, where γ is the RT growth rate (see Eq. 1 below). For bothg t=0.2 ns and 2.2 ns, note the distinct lack of higher order components to the perturbation spectral composition. Late in time, the perturbation has evolved into the nonlinear regime, and the bubble-and-spike shape shown edge-on in Fig. 2 is now observed face-on in the ln(Exposure) profile at 4.2 ns. The departure from a pure sinusoidal shape is now reflected in the appearance of higher order components (k=2-5) in the Fourier spectrum. The rate opf growth of the perturbation changes as well v ith the transition to the nonlinear regime. The asymptotic limit is bubble growth that is linear in time due to terminal bubble velocity[Layzer ref] and spike growth that is quadratic in time due to the spikes approaching freefall. High quality measurements of perturbation growth well into the nonlinear regime are somewhat hampered because a large amount of material is packed into a long, narrow spike. Finite instrumental spatial resolution makes this spike difficult to see, and its inflight alignment relative to the diagnostic could be problematical.

Measurements of RT evolution in the linear regime are critical, because it is during this phase that perturbations are growing exponentially

in time. We show in Fig. 4a a streaked image of a FS foil with a λ = 50 μm, η_0 = 0.8 μm sinusoidal perturbation in face-on geometry. The fundamental Fourier coefficient, corresponding to λ = 50 μm, of ln(Exposure) modulation is shown as a function of time in Fig. 3b, along with the result from 2D LASNEX simulations. The exponential growth phase lastws for essentially the entire extent of the drive, making this a good candidate for studying RT growth in the linear regime. The data in Fig. 4b is reproduced from Ref. 4, but the simulation is new. The drive modeling now uses the time-dependent laser power (as opposed to a generic shape scaled by the total laser energy[4,5]), "first-principles" opacities (see below), and the hohlraum emission (with its *ad hoc* multiplier of 6) is replaced by the calculated thermal self emission at the ablation front of the foil. Figure 4c is similar only for a CH(Br) foil with a λ = 50 μm, η_0 = 0.5 μm initial perturbation. We have not attempted to deconvolve the various instrument effects from the data, but rather include the measured 22X MTF, reflectance, and baclighter spectrum into the simulations. The measured 22X depth of field,[8] ~1000 μm, is large compared to the distance traveled by the foil, ~200 μm, so the MTF is assumed to remain constant throughout the foil acceleration in the face-on experiments.

Opacities enter the simulations in a critical way, since the amount of optical depth (OD) contained in the hot ablated plasma determines how much x-ray drive actually reaches the ablation front to accelerate the foil. In an effort to minimize uncertainties in plasma opacities, large lookup tables have been generated using the super transition array (STA)[13] and OPAL[14] opacity models. The STA model is based on a JJ coupling scheme, and is most appropriate for mid- to high-Z elements. The OPAL model is based on an LS coupling scheme, and explicitly sums over each individual atomic configuration, including term splitting. This model is best suited for

lighter elements, due to the computational time required as Z increases. There have been no *ad hoc* adjustment of any parameters in these opacity calculations, and the two models lead to very similar foil accelerations. For convenience, all calculations shown have used the STA opacities.

To illustrate the subtle differences in the hydrodynamic behavior of foils of FS versus CH(Br), we plot in Fig. 4d an estimated growth rate, γ, versus perturbation wavelength, λ. To do this we use a simple dispersion formula,[15]

$$\gamma = [Akg/(1+kL)]^{1/2} - \beta k v_a , \qquad (1)$$

whose time-dependent parameters (A, g, L, β, v_a) have been determined by comparing with the simulations. Here A is the Atwood number, $k=2\pi/\lambda$ is the perturbation wave number, L is the density gradient scale length, v_a is the ablation velocity, and β is an arbitrary multiplier on the convective stabilization term and takes a value between 1 and 2 for our indirect-drive experiments. The admixture of opacities in FS serves as a more effective preheat shield over a broader range of $\Delta(h\nu)$ than the L-band of Br in CH(Br). Hence, compared to FS the high energy tail of the drive x-rays in CH(Br) causes more volume heating, lowering ρ ("decompression"), increasing L, and for the same $\dot{m}$ increasing $v_a \propto \dot{m}/\rho$. This combination of slightly larger ablation velocity and gentler density gradient (larger L) at the ablation front for CH(Br) leads to a lower overall growth rate and a higher short-wavelength cutoff than FS. For reference we also show the expected classical growth rate for ideal, incompressible fluids, namely, $\lambda_{cl}=(Akg)^{1/2}$. The departure from classical for ablative growth is quite dramatic, especially at short wavelengths. Note that the details of this dispersion curve can be adjusted by modifying the amount and type of dopants in the foils.

IV. TWO-MODE EXPERIMENTS

When multiple modes are present in an initial perturbation, the behavior in the nonlinear regime is much more complex than for single modes. In addition to the bubble-and-spike formation described above, there is coupling between modes, say, k_i and k_j, to spawn new modes of waveneumber $k_i \pm k_j$. Theoretical work suggests that the growth of one mode may be substantially altered by the presence of another,[16] and that the overall saturation level of complex perturbations may be affected.[17] We have done two-mode experiments to have a first look at these effects.

The mold used to impose the initial 2λ perturbation on a CH(Br) foil is shown in Fig. 5a: $\lambda_{1,2}$ = 50, 75 μm with η_o = 2 μm for each. A ln(Exposure) profile at 2.7 ns is also shown. The Fourier coefficientsof Δln(Exposure) for the two pre-existing modes, $\lambda_{1,2}$ = 50, 75 μm, are shown as a function of time in Fig. 5b. The Fourier coefficients for the $k_1 \pm k_2$ coupled modes, corresponding to wavelengths of 30 μm and 150 μm, are observed only after the RT instability has entered the nonlinear regime, as shown in Fig. 5c. That the λ = 30 μm and 150 μm modes were not present initially was verified both by measuring the spatial amplitudes on the foil directly with contact profilometry and by radiographing a 2λ foil on a DC x-ray source. The solid curves correspond to the LASNEX simulations of the 2λ experiment. Though the agreement is reasonable, the simulations apperar to evolve slightly faster than the data, an effect that is not yet fully understood. We also show with the dashed curves in Fig. 5b the result we would have expected if only the λ = 75 μm or the λ = 50 μm perturbation had been present alone, based on the simulations. It is evident that in the nonlinear regime of the 2λ case, the evolution of mode k_1 is affected by the presence of mode k_2, and vice versa. We emphasize, however, that the overall perturbation growth is not necessarily retarded, but rather redistributed via mode coupling into a broader Fourier spectrum

corresponding to a stronger change of shape. This is illustrated in Fig. 5d with a comparison of the shapes of the ln(Exposure) profiles corresponding to the calculations shown in Fig. 5b.

V. SURFACE-FINISH EXPERIMENTS

The only conclusive test of how a perturbation consisting of a full continuum of modes evolves at the ablation front is to actually impose such a perturbation and measure its evolution. Even though recent progress has been made in developing 3D modeling capability,[18] a complete model including radiation transport is not yet at hand. Nevertheless, the gross features of growth, coupling, and saturation with a broad spectrum of initial modes can be looked at experimentally. Hence we have started a series of 3D surface finish experiments, and present our initial results here. A CH(Br) foil with a rough surface of characteristic perturbation $\langle\eta_0\rangle \approx 2\pm1$ μm imposed on it was accelerated and imaged face-on with a gated x-ray framing camera.[10] Typical 2D images taken at 2.0, 3.2, and 4.4 ns are shown in Fig. 6a. It is evident directly from the images that late in time the surface has evolved into large, roughly hexagonal bubbles of size ~100 μm. This is quantified by the Δln(Exposure) ≈ -ΔOD profiles shown in Fig. 6b. The peak-to-valley maximum δOD late in time (4.4 ns) of the largest bubble-and-spike feature is δOD ≈ 1.5, which exceeds the original optical depth, OD_0, of the entire foil. For comparison, we show in Fig. 6c similar profiles for a smooth foil of characteristic surface roughness $\langle\eta_0\rangle \approx 3.5$ μm. There is no obvious growth into bubbles and spikes. Measurements of the initial surface finish of comparable foils are shown in Fig. 6c. Adopting an operational definition of foil "break up" as occurring when $\delta OD > OD_0$, we conclude that our nominal smooth foils remain intact throughout whereas foils imposed with a very rough initial surface finish break up late in time. The Fourier transforms corresponding to the optical depth profiles of Figs. 6b,c are given in Figs.

6d,e. For the rough surface, the growth late in time is dominated by modes k = 3-8 corresponding to $\lambda \approx 150$-50 μm. The Fourier data for the smooth foil show no significant growth. These initial results are only qualitative, and we are currently in the process of doing a more in depth analysis of the coupling and saturation effects for this broad spectrum of initial modes. Development of a 3D modeling capability is also in progress.

VI. CONCLUSION AND SUMMARY

In conclusion, we have done an extensive series of experiments accelerating FS foils and CH(Br) foils by x-ray ablation using a shaped, low adiabat drive. The RT-induced perturbation growth was studied by imposing single-mode and multi-mode sinusoidal initial perturbations, and also by accelerating a foil with a rough surface finish. We use our single-mode experiments along with foil trajectory experiments to develop a modeling capability, then use the simulations to illustrate the subtle differences in behavior between FS and CH(Br) foils, with the latter being slightly less RT unstable. Clear evidence of mode coupling is seen in the multi-mode experiments, with the $k_i \pm k_j$ coupled modes being spawned in the nonlinear regime. This leads to a change in shape of the perturbation, resulting in a general broadening of the Fourier spectrum. Very recent surface finish experiments qualitatively show that smooth foils remain intact whereas foils with a very rough surface finish break up. We will be examining in the near future the details of exactly how multiple modes evolve differently than single modes, with particular attention paid to saturation effects.

It is a pleasure to acknowledge the assistance of R. Kauffman, H. Kornblum, J. Moreno, and T. Peyser with backlighter spectroscopy measurements, the technical support of J. Oertel and LANL in running the

gated x-ray framing camera, and the dedicated staff and support personnel at Nova. This work was performed under the auspices of the U.S. DOE by the Lawrence Livermore National Laboratory under contract number W-7405-ENG-48.

References:

[1]S. Chandrasekhar, *Hydrodynamic and Hydromagnetic Stability* (Oxford U.P., London, 1968), Chap. 10.

[2]J.D. Lindl and W.C. Mead, Phys. Rev. Lett. **34**, 1273 (1975); H. Sakagami and K. Hishihara, Phys. Fluids B **2**, 2715 (1990).

[3]J. Grun, M.E. Emery, C.K. Manka, T.N. Lee, E.A. McLean, A. Mostovych, J. Stamper, S. Bodner, S.P. Obenshain, and B.H. Ripin, Phys. Rev. Lett. **58**, 2672 (1987); M. Desselberger, O. Willi, M. Savage, and M. Lamb, Phys. Rev. Lett. **65**, 2997 (1990); S.G. Glendinning, S.V. Weber, P. Bell, L.B. DaSilva, S.N. Dixit, M.A. Henesian, D.R. Kania, J.D. Kilkenny, H.T. Powell, R.J. Wallace, P.J. Wegner, J.P. Knauer, and C.P. Verdon, Phys. Rev. Lett. **69**, 1201 (1992).

[4]B.A. Remington, S.W. Haan, S.G. Glendinning, J.D. Kilkenny, D.H. Munro, and R. Wallace, Phys. Rev. Lett. **67**, 3259 (1991).

[5]B.A. Remington, S.W. Haan, S.G. Glendinning, J.D. Kilkenny, D.H. Munro, and R. Wallace, Phys. Fluids B **4**, 967 (1992).

[6]J.D. Kilkenny, Phys. Fluids **2**, 1400 (1990).

[7]R.J. Ellis, J.E. Trebes, D.W. Phillion, J.D. Kilkenny, S.G. Glendinning, J.D. Wiedwald, and R.A. Levesque, Rev. Sci. Instrum. **61**, 2759 (1990) and references therein.

[8]B.A. Remington, S.G. Glendinning, R.J. Wallace, S. Rothman, R. Morales, Rev. Sci. Instrum. **63**, 5080 (1992).

[9]B.A. Remington, B.A. Hammel, O.L. Landen, and R.A. Pasha, Rev. Sci. Instrum., Rev. Sci. Instrum. **63**, 5083 (1992).

[10]P.M. Bell, J.D. Kilkenny, O.L. Landen, R.L. Hanks, and D.K. Bradley, Rev. Sci. Instrum **63**, 5073 (1992); J. Oertel, B. Watt, T. Archuleta, J. Jimerson, J. Wiedwald, P. Bell, and R. Hanks, Bull. Am. Phys. Soc. **37**, 1522 (1992).

[11]E.M. Campbell, Laser and Part. Beams **9**, 209 (1991); E.M. Campbell, J.T. Hunt, E.S. Bliss, D.R. Speck, and R.P. Drake, Rev. Sci. Instrum. **57**, 2101 (1986).

[12]G.B. Zimmerman and W.L. Kruer, Comments Plasma Phys. Controlled Fusion **11**, 51 (1975).

[13]A. Bar-Shalom, J. Oreg, W.H. Goldstein, D. Shvarts, and A. Zigler, Phys. Rev. A **40**, 3183 (1989).

[14]C.A. Iglesias, F.J. Rogers, and B.G. Wilson, Ap. J. **397**, 717 (1992); *ibid* **360**, 221 (1990); *ibid* **322**, L45 (1987); F.J. Rogers and C.A. Iglesias, Ap. J. Suppl. **79**, 507 (1992).

[15]H. Takabe, L. Montierth, and R.L. Morse, Phys. Fluids 26,2299 (1983); H. Takabe, K. Mima, L. Montierth, and R.L. Morse, ibid **28**, 3676 (1985); D.H. Munro, Phys. Rev. A **38**, 1433 (1988).

[16]J.P. Dahlburg, J.H. Gardner, and M.H. Emery, Bull. Am. Phys. Soc. **35**, 1969 (1990, Abstract 3E3); D. Ofer, D. Shvarts, Z. Zinamon, S.A. Orszag, Phys. Fluids B **4**, 3549 (1992).

[17]S.W. Haan, Phys. Rev. A **39**, 5812 (1989); *ibid*, Phys. Fluids B **3**, 2349 (1991).

[18]D.L. Youngs, Phys. Fluids A **3**, 1312 (1991); J.P. Dahlburg and J.H. Gardner, Phys. Rev. A **41**, 5695 (1990); R.J.P. Town and A.R. Bell, Phys. Rev. Lett. **67**, 1863 (1991); H. Sakagami and K. Nishihara, Phys. Rev. Lett. **65**, 432 (1990)

Figure Captions:

Figure 1. Setup for indirect-drive Rayleigh-Taylor experiments. (a) Schematic of the experimental setup (not to scale). The foil is mounted on the front wall of a cylindrical gold hohlraum with surface perturbation facing inwards, and drive beams entering the ends of the hohlraum generate an approximately thermal x-ray drive. A separate laser beam striking a backlighter disk generates a back illumination of x-rays at higher frequency but much lower flux. (b) The solid curves give the power versus time of the eight 1/3 μm drive laser beams. The dotted curve gives the power and relative timing of the 0.528 μm backlighter beam. (c) Typical unprocessed 1D image (in film density) of a 1D foil trajectory measurement using a streaked-slit x-ray imager filtered with 875 μm of Be and a large area (750 μm diameter) Fe backlighter. (d) Analyzed result of three such trajectory shots, along with the result of a 1D LASNEX simulation. The suares correspond to two shots taken with the 22X using a Rh backlighter, and the solid points correspond to the image in (c).

Figure 2. Results of a perturbation growth experiment with a FS foil with λ=100 μm, η_0=4.6 μm initial sinusoidal perturbation, viewed side-on with a ~350 μm diameter Fe backlighter from an RPP-smoothed laser beam. The diagnostic, a gated x-ray pinhole imager, was run at 12x magnification with 10 μm pinholes, and a 381 μm Be filter. The ablation front corresponds to the lower side of the foil in the images, and the images correspond to times of (a) 2.0 ns, (b) 3.2 ns, and (c) 4.4 ns. (d) An isodensity contour plot from 2D LASNEX simulations at 4.4 ns.

Figure 3. Typical example of a measurement of perturbation growth using face-on radiography. (a) Streaked image for a CH(Br) foil with a λ = 100 μm, η_0=2.5 μm perturbation. (b) The corresponding modulated optical depth

profiles at three different times spanning the linear and nonlinear regimes. (c) Fourier decomposition of the profiles shown in (b) showing that the shape change in the nonlinear regime is reflected by the generation of higher harmonics, in this case the first 5 harmonics.

Figure 4. Face-on measurements of growth in the linear regime for two different foil materials, using the streaked 22X microscope with a ~700 μm diameter backlighter x-ray spot. (a) Raw 1D image of the evolution of a FS foil with a λ = 50 μm, η_0=0.8 μm sinusoidal initial perturbation. The vertical extent of the image corresponds to the 5 ns backlighter duration. (b) Coefficients of the fundamental mode of Δln(Exposure). The backlighter was Rh and a 25 μm Be filter was used. (c) Same only for a CH(Br) foil with a λ = 50 μm, η_0 = 0.5 μm initial perturbation. The backlighter was Mo and the filters used were 25 μm Be and 25 μm mylar. The smooth curves are the results of 2D LASNEX simulations, including the effect of the instrument MTF. The starting time, t=0, corresponds to the start of the drive lasers. (d) Fitting a simple dispersion relation to results of the simulations, we then can plot for a given acceleration, g = 60 μm/ns^2, the growth rate versus perturbation wavelength λ for the two foil materials, as compared to the classical result. The effect of ablation is to cause a short-λ cutoff, with the cutoff occurring at a larger λ for CH(Br) compared to FS.

Figure 5. Results of 2-mode (2λ) experiments and simulations for a foil with λ_1, λ_2 = 50, 75 μm, η_0=2.0 μm. (a) The mold used in making the foils, and a Δln(Exposure) profile at 2.7 ns. The full time dependence is shown in (b). The measurements were made with the streaked 22X filtered with 25 μm Be and 25 μm mylar and a ~700 μm diameter Rh backlighter. (b) Fourier coefficients of Δln(Exposure) for the two pre-existing modes, compared with the results of 2D LASNEX simulations for the 2λ case (solid curves) versus calculations where either the λ = 50 μm perturbation or the λ = 75 μm

perturbation were present alone, "1λ calc" (dashed curves). (c) The two coupled modes are shown along with the results of the simulations (solid curves). (d) Comparison of the simulated ln(Exposure) profiles from the 2λ case versus treating the two individual perturbations separately then combining the net perturbation afterwards, neglecting mode coupling.

Figure 6. Results of surface-finish experiments using CH(Br) foils with two different surface finishes, backlit with an RPP-smoothed ~350 μm diameter Sc backlighter, and imaged with a gated x-ray framing camera filtered with 381 μm Be. (a) Typical 2D images at 2.0, 3.2, and 4.4 ns of an accelerated foil with a very rough surface finish. (b) Corresponding Δln(Exposure) profiles for the rough foil (left) and for a smooth foil (right). (c) Initial surface finish for the rough foil (left) and smooth foil (right). Note the factor of 100 difference in scales. (d) Fourier decomposition of the ln(Exposure) profiles shown in (b). (e) Same for the initial surface finish shown in (c).

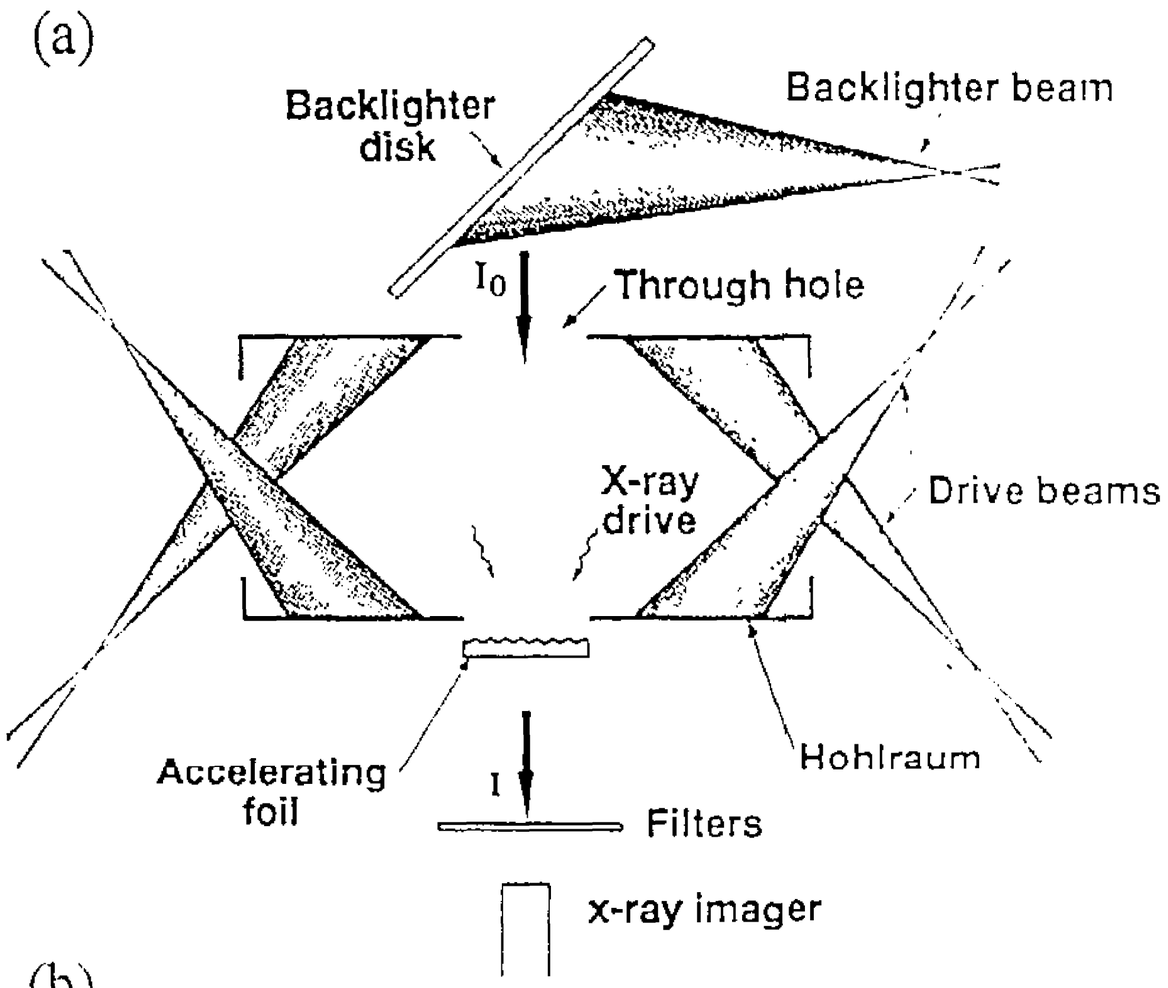
(a)
Backlighter disk
Backlighter beam
I_0
Through hole
X-ray drive
Drive beams
Accelerating foil
Hohlraum
I
Filters
x-ray imager

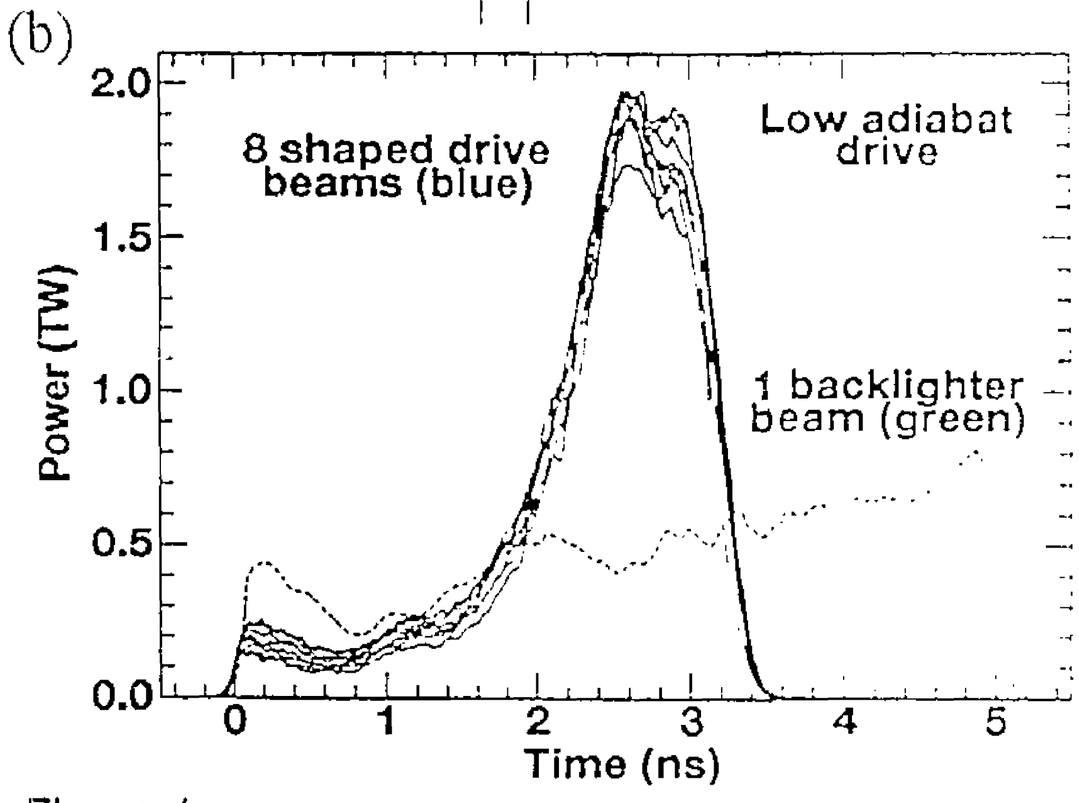
(b)
8 shaped drive beams (blue)
Low adiabat drive
1 backlighter beam (green)
Power (TW)
Time (ns)

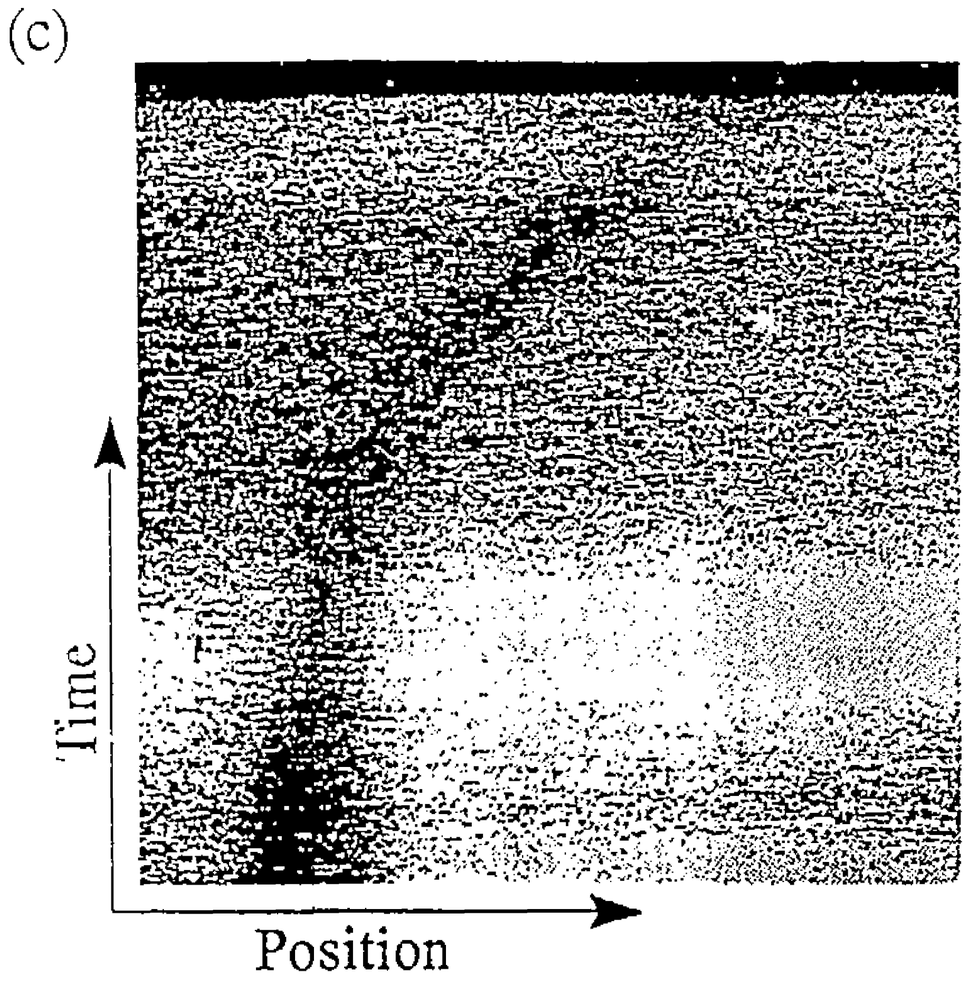
(c)
Time
Position

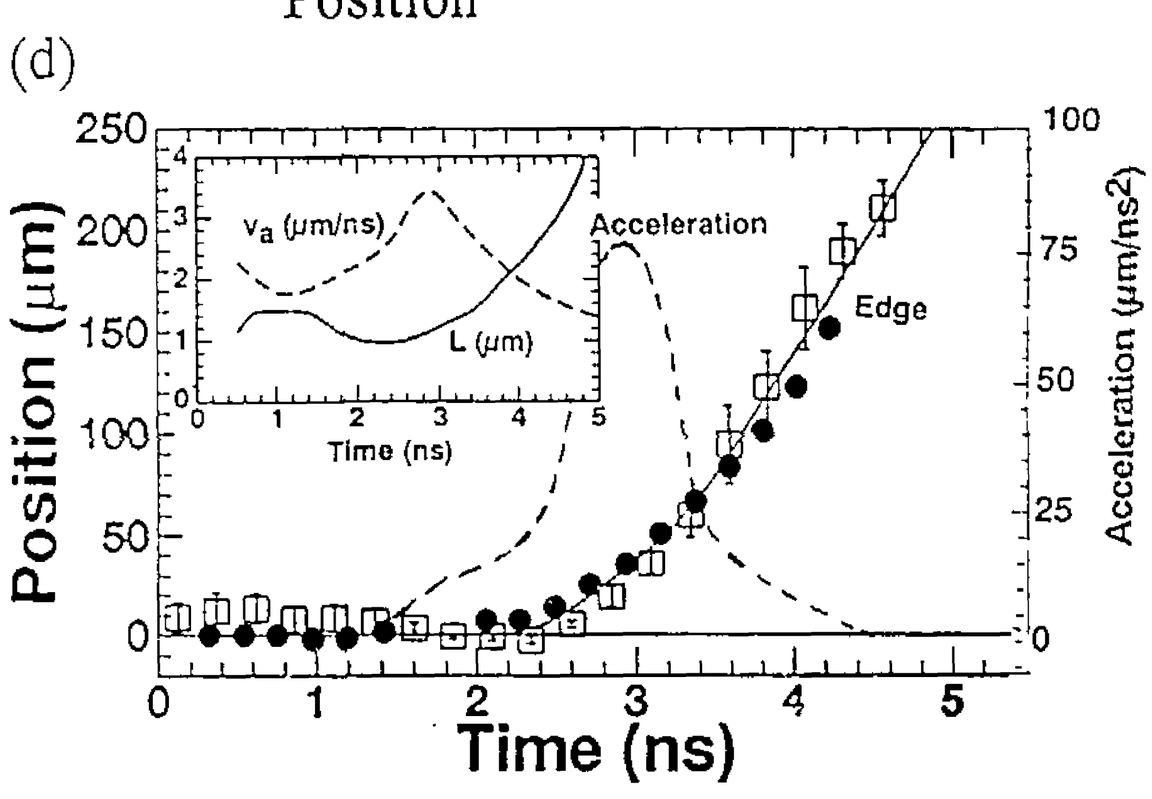
(d)
v_a (μm/ns)
L (μm)
Time (ns)
Acceleration
Edge
Position (μm)
Acceleration (μm/ns²)
Time (ns)

Figure 1

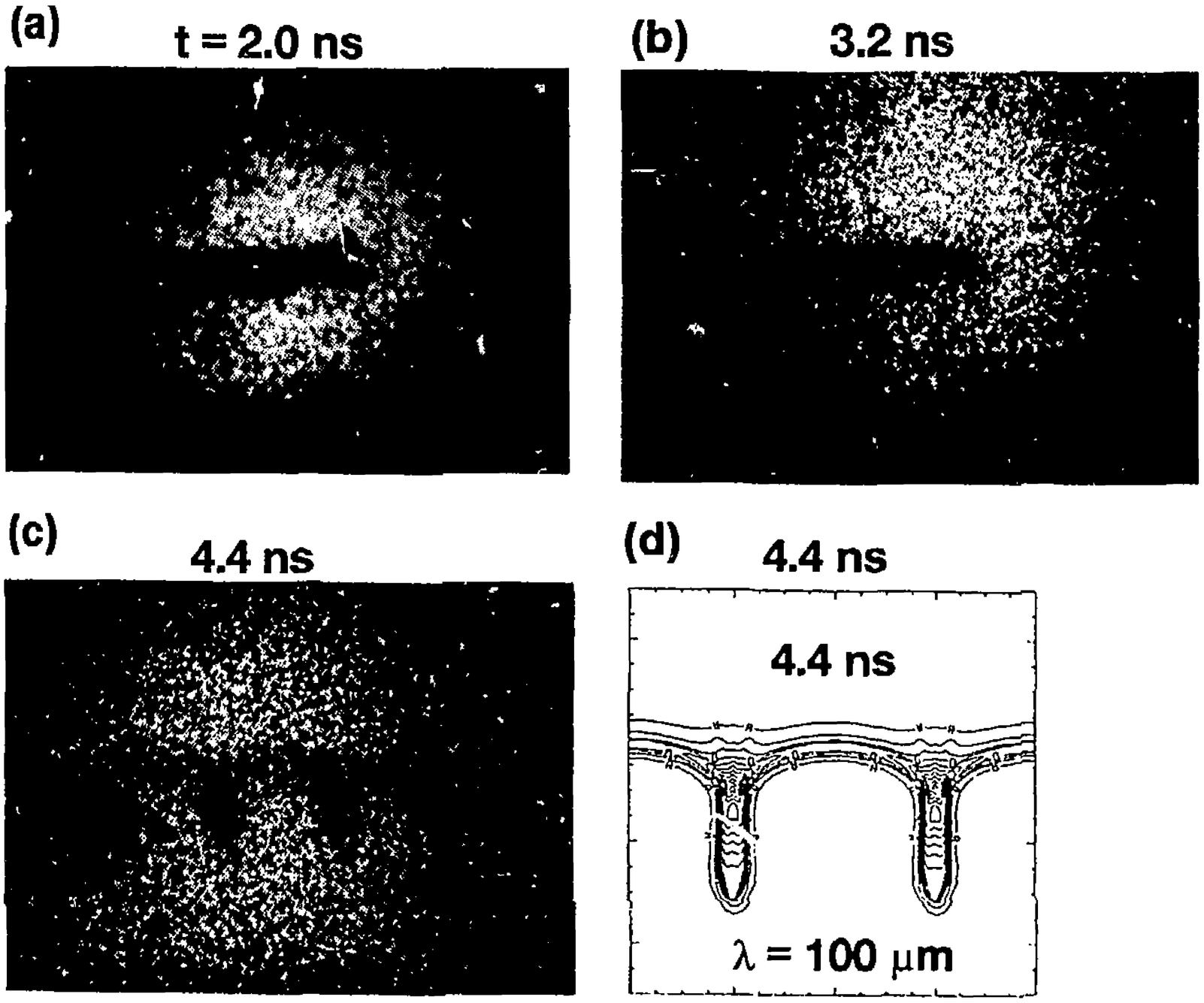
(a)
t = 2.0 ns
(b)
3.2 ns
(c)
4.4 ns
(d)
4.4 ns
4.4 ns
λ = 100 μm

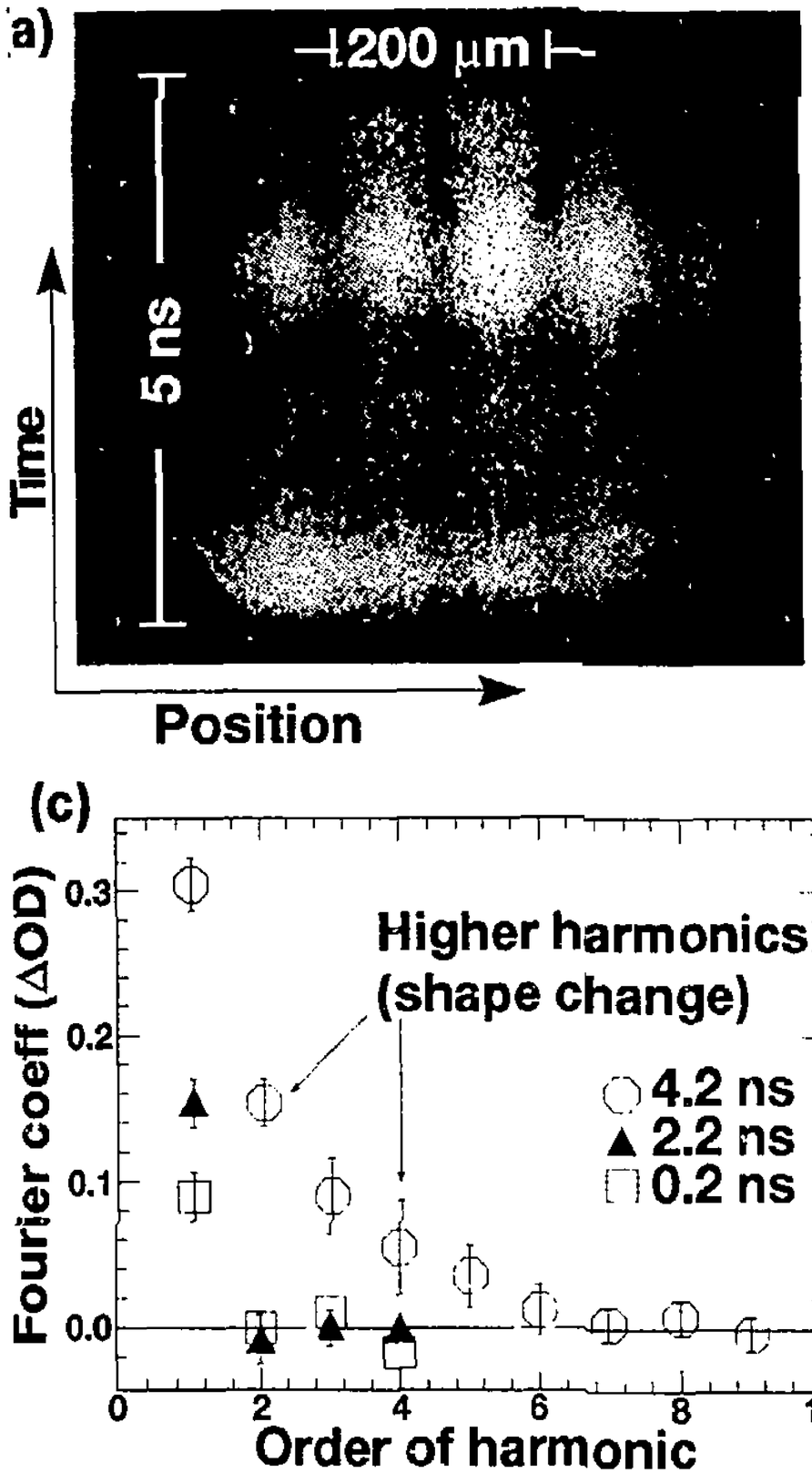
a)
200 μm
5 ns
Time
Position
(b)
CH (Br)
λ = 100 μm
η0 = 2.5 μm
Nonlinear regime
Spike
Bubble
4.2 ns
2.2 ns
Linear regime
0.2 ns
Δ (Optical depth)
1.5
1.0
0.5
0
0.5
0
0.5
0
0
100
200
300
Position (μm)
(c)
Fourier coeff (ΔOD)
0.3
0.2
0.1
0.0
Higher harmonics
(shape change)
4.2 ns
2.2 ns
0.2 ns
0
2
4
6
8
10
Order of harmonic

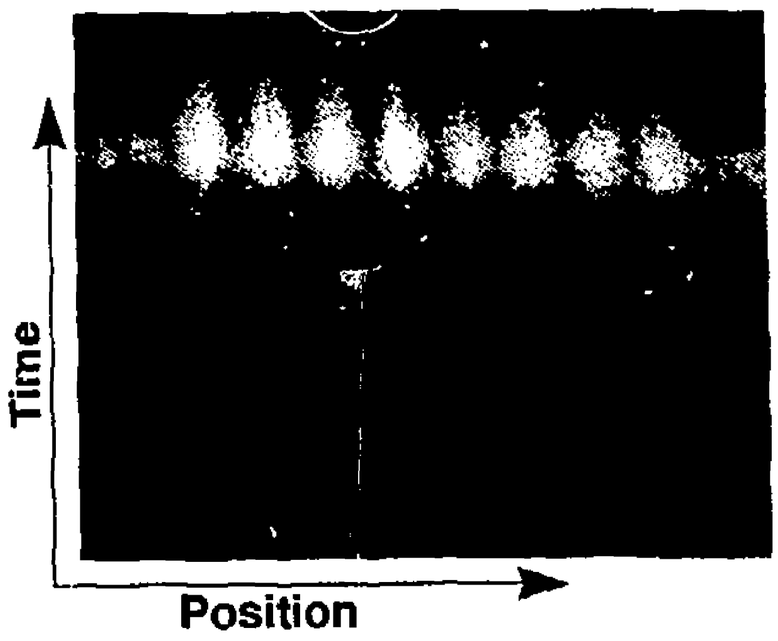
Time
Position

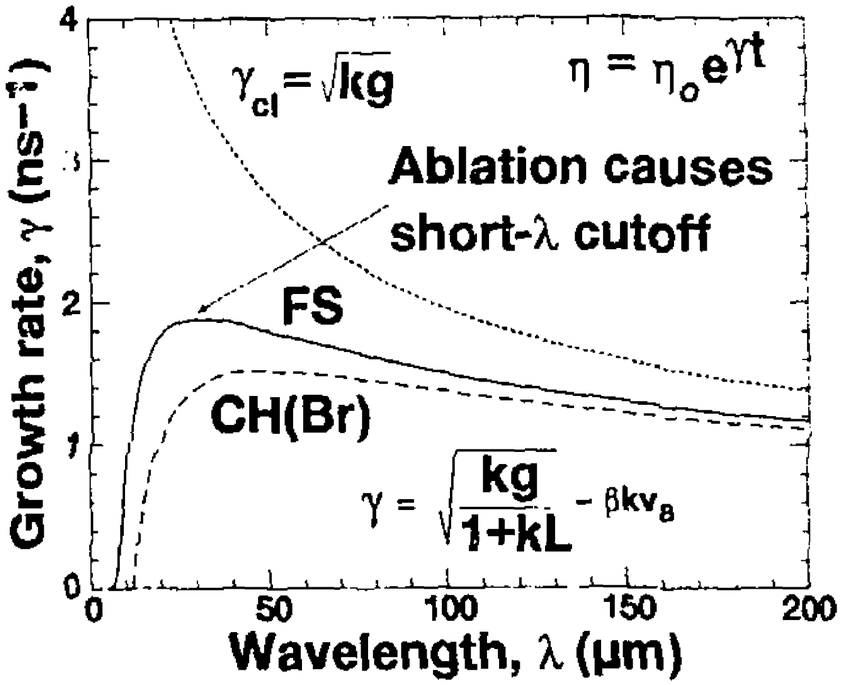
$\gamma_{cl} = \sqrt{kg}$
$\eta = \eta_o e^{\gamma t}$
Ablation causes
short-λ cutoff
FS
CH(Br)
$\gamma = \sqrt{\frac{kg}{1+kL}} - \beta k v_a$
Growth rate, γ (ns⁻¹)
Wavelength, λ (μm)
0
1
2
3
4
0
50
100
150
200

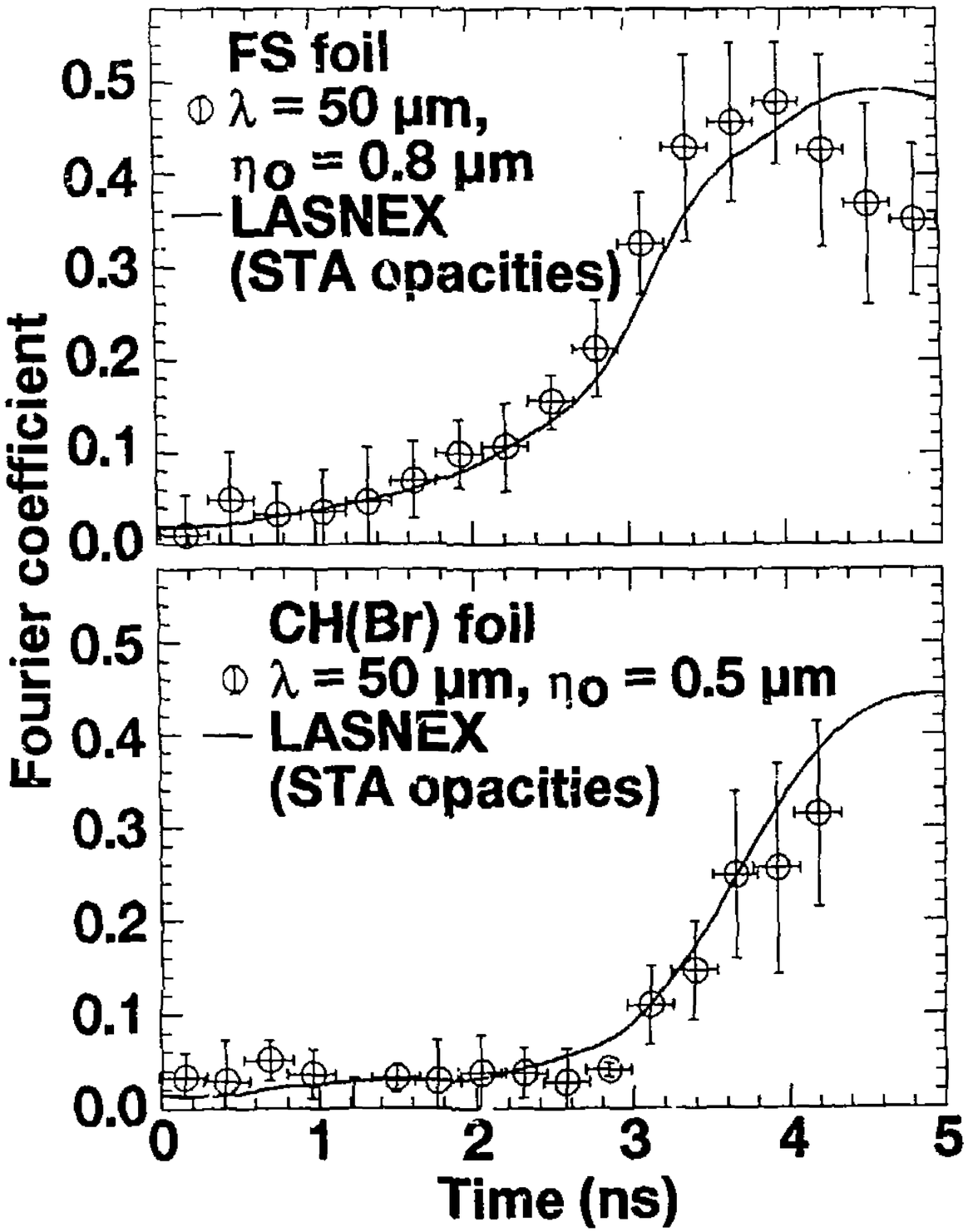
FS foil
λ = 50 μm,
η_o = 0.8 μm
LASNEX
(STA opacities)
CH(Br) foil
λ = 50 μm, η_o = 0.5 μm
LASNEX
(STA opacities)
Fourier coefficient
0.0
0.1
0.2
0.3
0.4
0.5
0
1
2
3
4
5
Time (ns)

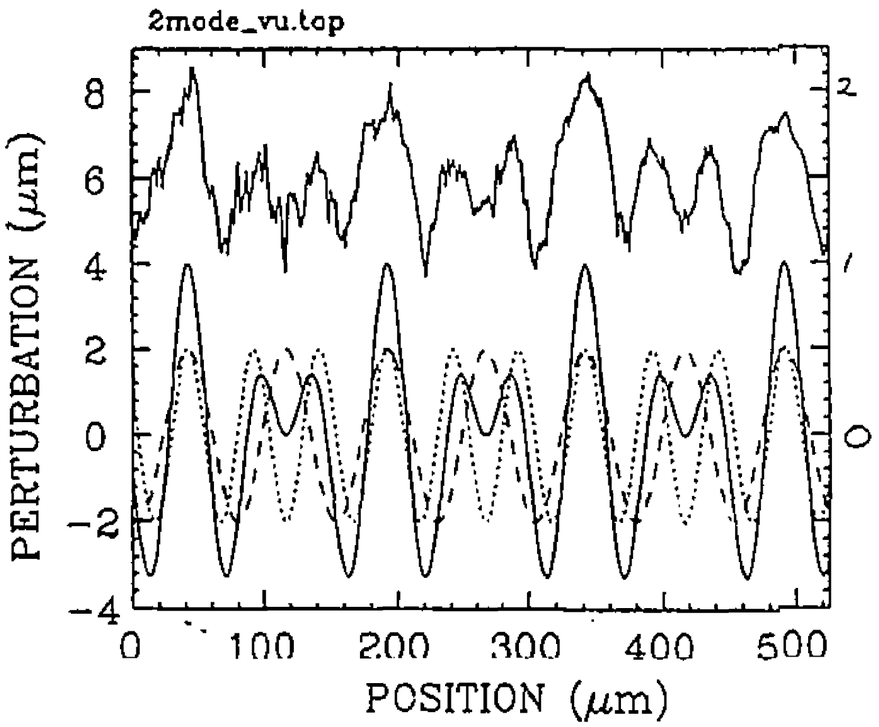

(b)

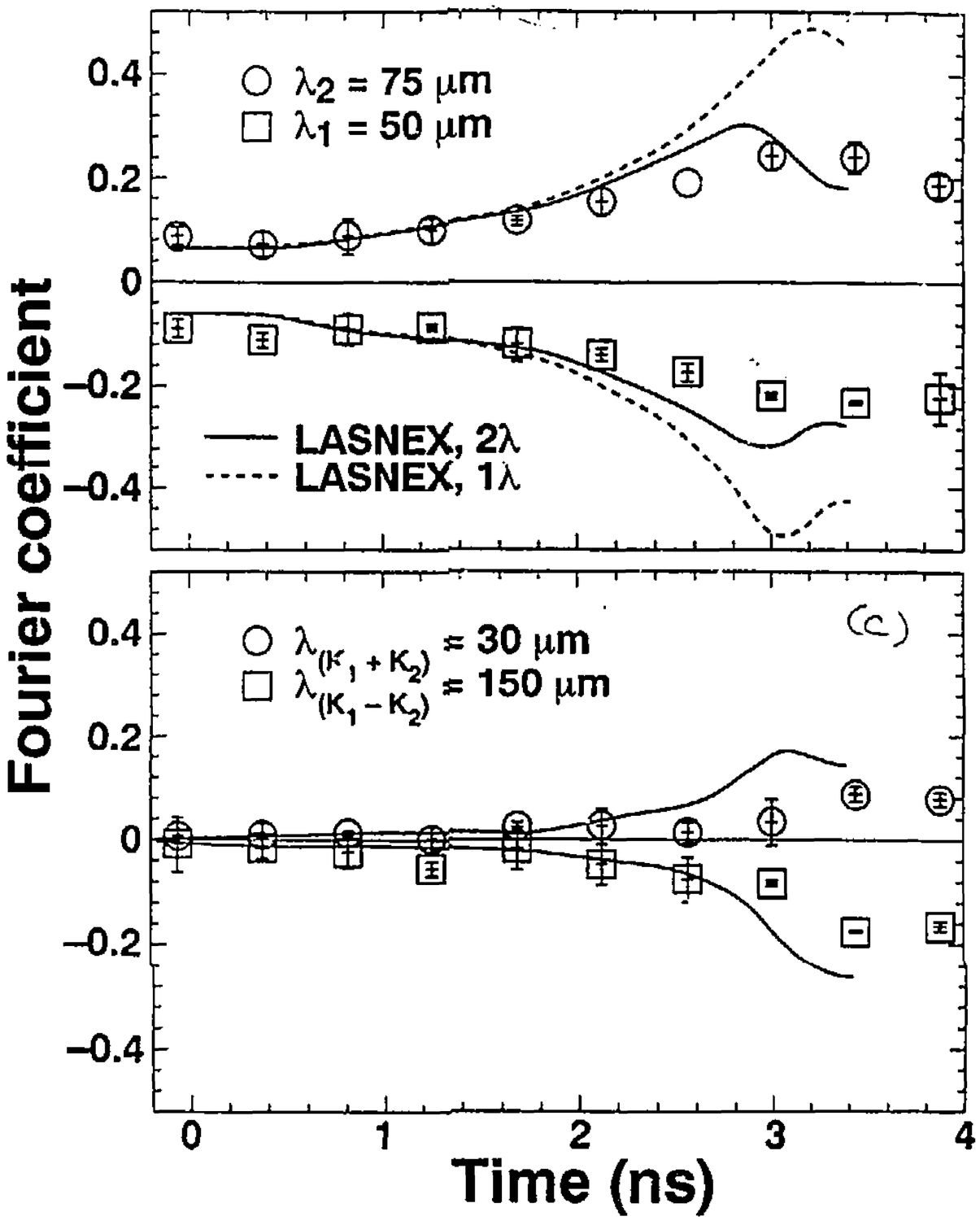

(c)

(d)

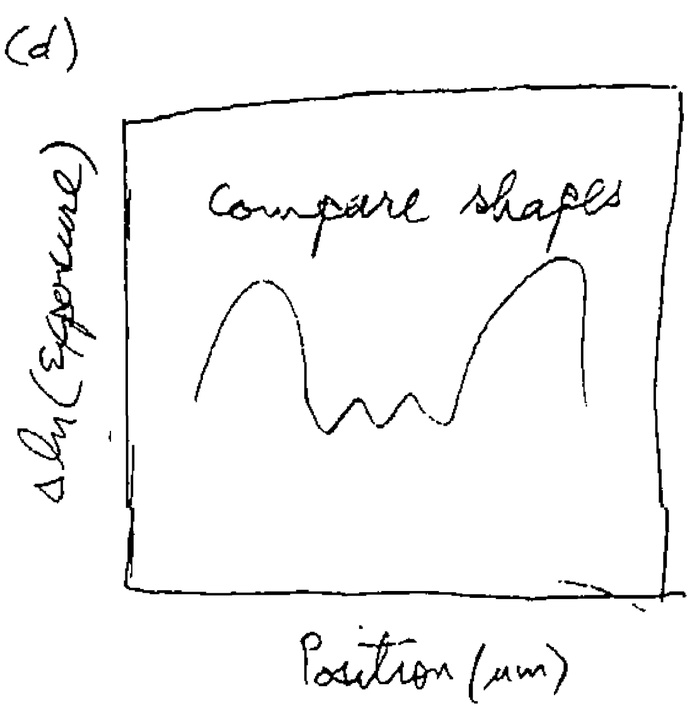

16×9 => 15

15 → 12.5 → 11

(a) **Rough foil:**

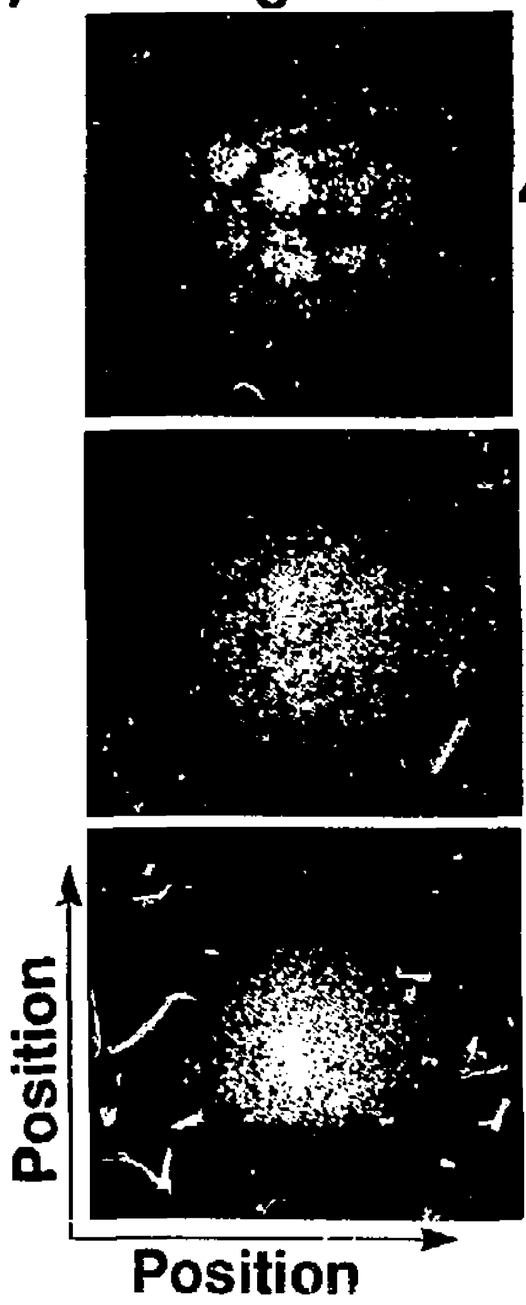
4.4 ns
3.2 ns
2.0 ns
Position
Position

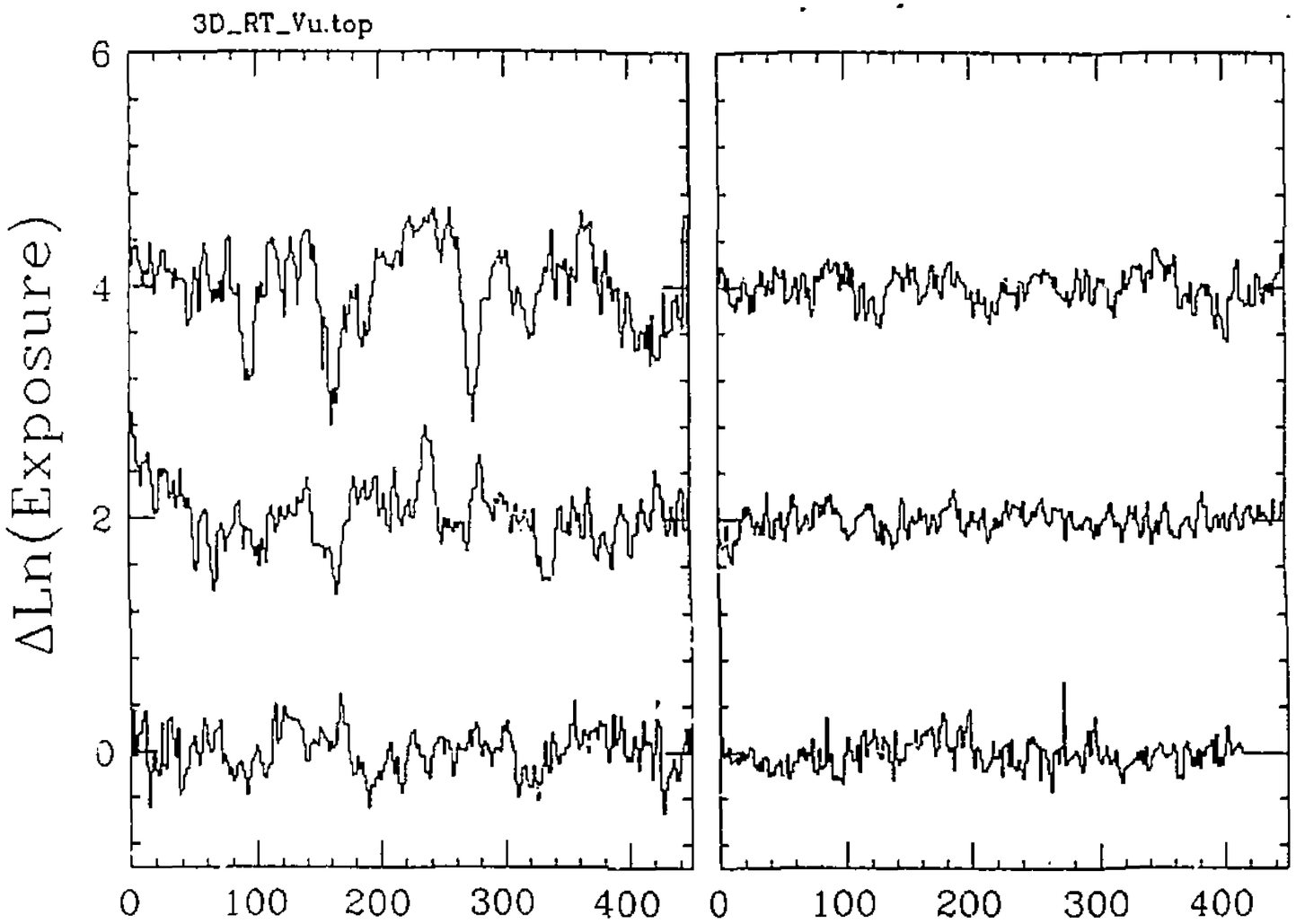
3D_RT_Vu.top
ΔLn(Exposure)
6
4
2
0
0
100
200
300
400
Position (μm)

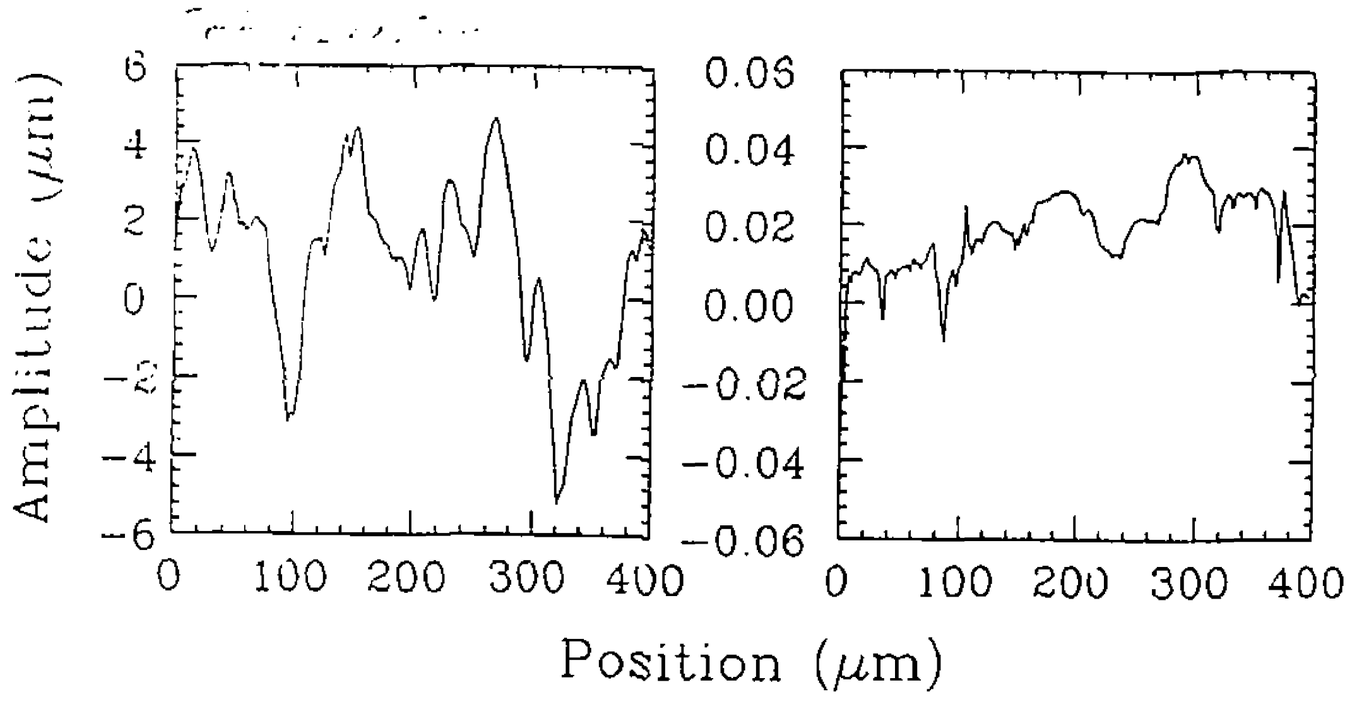
Amplitude (μm)
6
4
2
0
−2
−4
−6
0.06
0.04
0.02
0.00
−0.02
−0.04
−0.06
0
100
200
300
400
Position (μm)

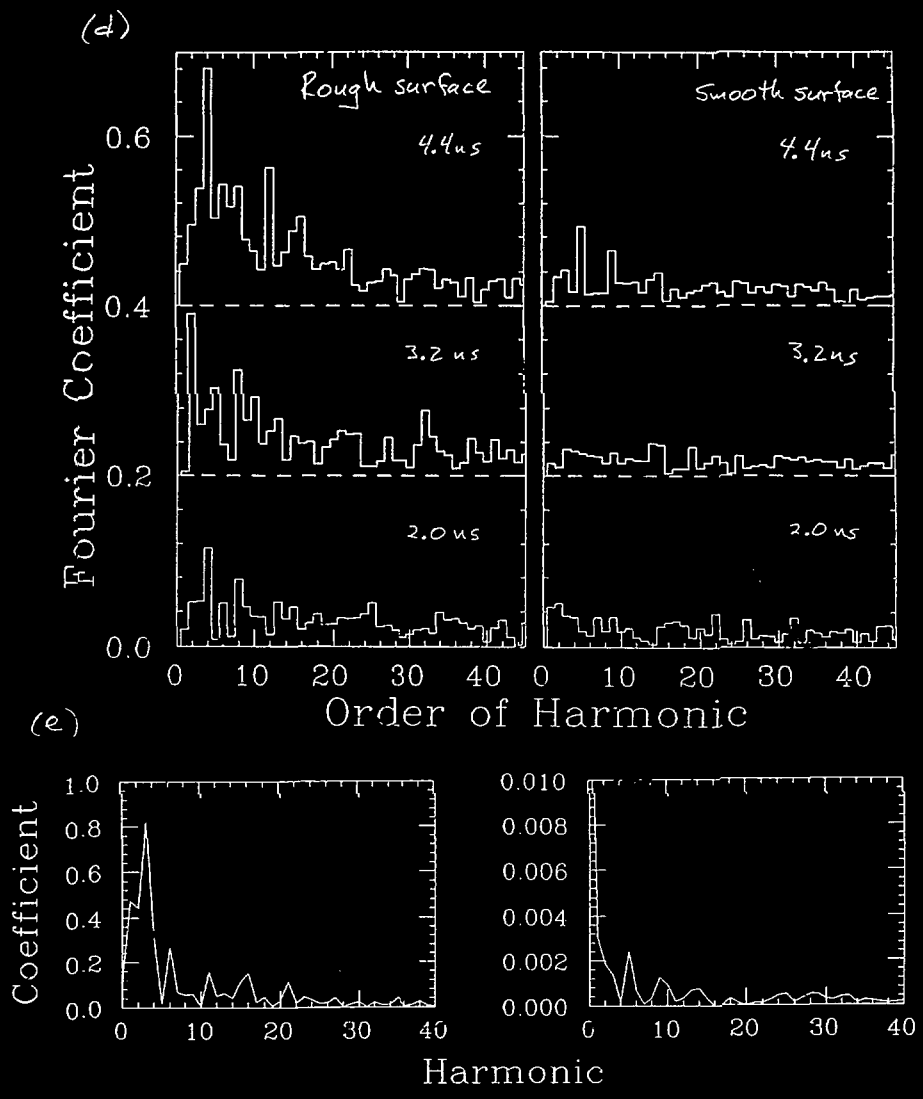
(d)
Rough surface
Smooth surface
4.4ns
3.2ns
2.0ns
Fourier Coefficient
0.0
0.2
0.4
0.6
0
10
20
30
40
Order of Harmonic
(e)
Coefficient
0.0
0.2
0.4
0.6
0.8
1.0
0.000
0.002
0.004
0.006
0.008
0.010
Harmonic

Fig. 6 cont.